NANO LETTERS

pubs.acs.org/NanoLett

Letter

Carbothermal Shock Synthesis of Lattice Oxygen-Mediated High-Entropy FeCoNiCuMo-O Electrocatalyst with a Fast Kinetic, High Efficiency, and Stable Oxygen Evolution Reaction

Wanyi Liao, Fangzhu Qing,* Qian Liu, Rongxuan Wu, Congli Zhou, Lina Chen, Yuanfu Chen,* and Xuesong Li*

Cite This: https://doi.org/10.1021/acs.nanolett.4c05658

Read Online

ACCESS | Metrics & More | Article Recommendations | Supporting Information

ABSTRACT: Efficient oxygen evolution reaction (OER) catalysts with fast kinetics, high efficiency, and stability are essential for scalable green production of hydrogen. The rational design and fabrication of catalysts play a decisive role in their catalytic behavior. This work presents a high-entropy catalyst, FeCoNiCuMo-O, synthesized via carbothermal shock. Synergistic optimization of the adsorption evolution mechanism (AEM) and lattice oxygen mechanism (LOM) was realized and demonstrated through the combination of *in situ* spectra/mass spectrometry and chemical probe analysis in FeCoNiCuMo-O. Furthermore, the robust stability is reinforced by the inherent properties conferred by the high-entropy design. The catalyst exhibits outstanding performance metrics, featuring an exceptionally low Tafel slope of 41 mV dec^{-1}, a low overpotential of 272 mV at 10 mA cm^{-2}, and a commendable endurance (a mere 2.2% voltage decline after a 240-h continuous chronopotentiometry test at 10 mA cm^{-2}). This study advances the development of efficient, durable OER electrocatalysts for sustainable hydrogen production.

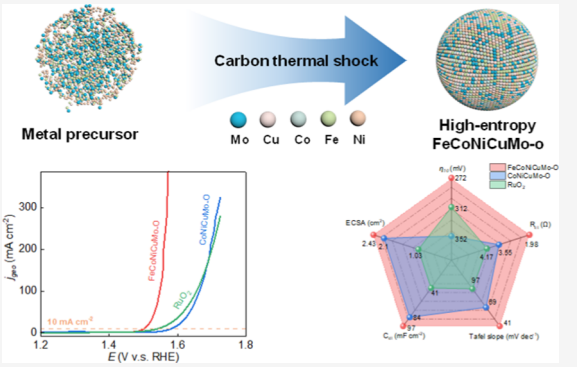

KEYWORDS: *carbothermal shock, OER, LOM, high entropy, electrocatalysis*

Global efforts to combat climate change have driven the demand for low-carbon and zero-carbon technologies.[1,2] Prominent among these is the harnessing of water electrolysis for hydrogen generation, especially when powered by renewable energy resources, enabling carbon-neutral outcomes vital for the decarbonization of industries, transportation networks, and power systems.[3] In the process of water electrolysis, the efficiency of the oxygen evolution reaction (OER) directly impacts the overall energy consumption and economic value.[4] This process is typically associated with high reaction energy barriers and overpotentials, necessitating the use of efficient catalysts to enhance the reaction rates.[5] Although noble metals initially served as reliable catalysts, their exorbitant costs and finite reserves prompted a shift toward exploring alternatives grounded in abundant transition metals like iron, cobalt, and nickel, valued for their economic accessibility and widespread availability.[6−9] However, these novel catalysts remain challenging with persistent issues concerning performance efficiency and durability.[10] The traditional understanding of the OER mechanism has primarily focused on the adsorbate evolution mechanism (AEM). According to AEM, changing the Gibbs free energy of one intermediate will linearly affect the counterpart of other intermediates (i.e., $\Delta G_{*OOH} = \Delta G_{*OH} + 3.0 \pm 0.2$ eV).[10−13] Consequently, it is impossible to simultaneously optimize the Gibbs free energies of all intermediates to achieve optimal reaction conditions. Even with material design and structural optimization partially addressing these conflicts, it remains challenging to completely overcome the limitations imposed by the linear relationship.[2,14,15] Recent advancements have unveiled the lattice oxygen mechanism (LOM), distinguishing itself by involving lattice oxygen directly in the OER, rather than surface-adsorbed intermediates, in the formation of O−O bonds.[10,16,17] This breaks free from AEM's linear constraints and paves the way for high activity and fast kenitics.[18] However, it requires rational regulation of the catalyst's electronic structure to facilitate lattice oxygen activation. Moreover, the dynamic nature of lattice oxygen engagement, entailing rapid oxygen migration and transient vacancy creation, can compromise material integrity and longevity.[19,20]

Irrespective of whether AEM or LOM dominates, the adsorption and desorption of intermediates at active sites result

Received: November 11, 2024
Revised: December 28, 2024
Accepted: December 30, 2024

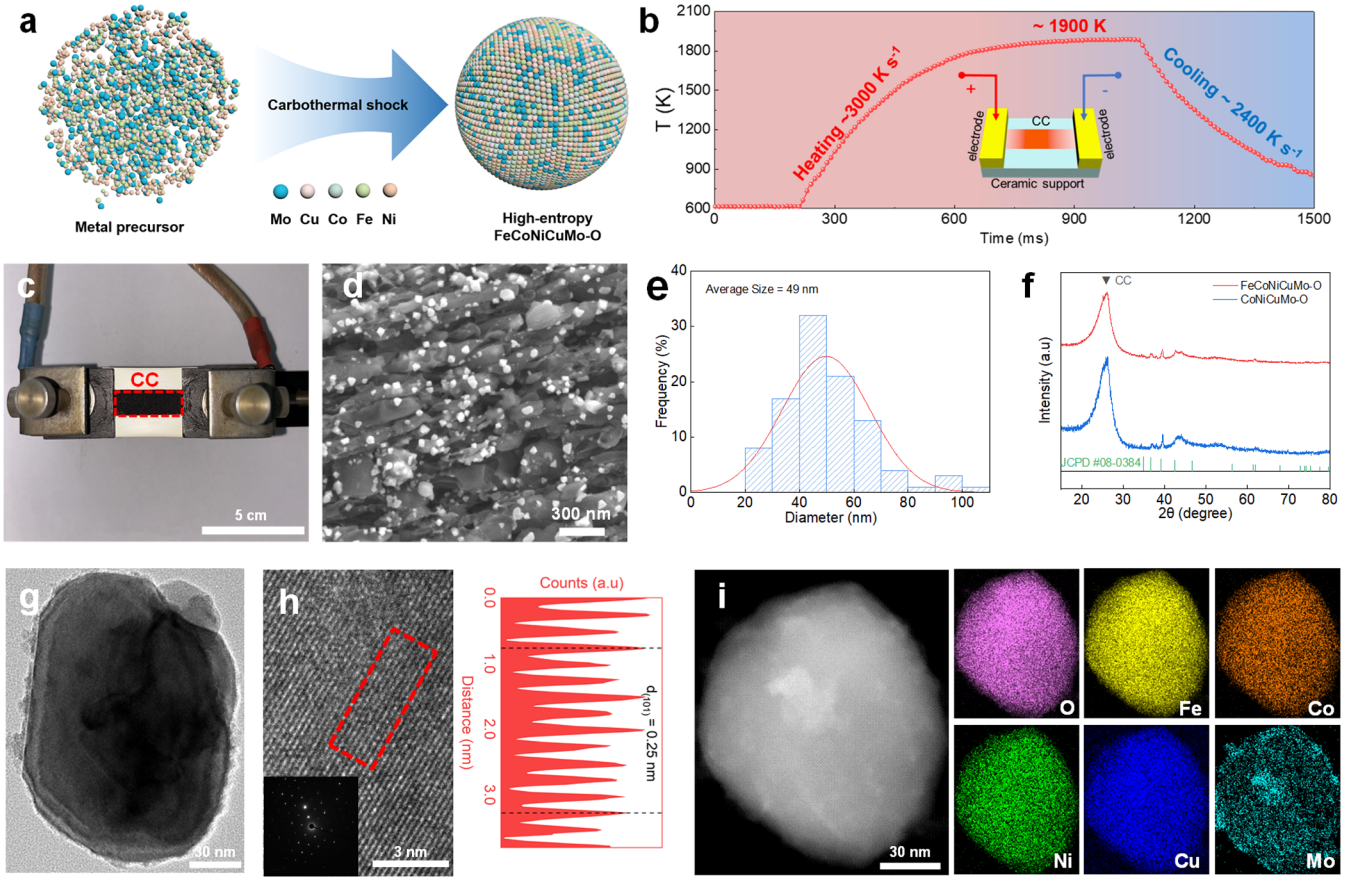

Figure 1. Preparation and morphology of FeCoNiCuMo-O. **a**. Scheme illustration for the thermodynamic induced evolution of FeCoNiCuMo-O. **b**. Temperature profile of CC during carbon thermal shock process (inset pattern: schematic diagram of the device). **c**. Photo of carbothermal shock device. **d**. High magnification SEM of FeCoNiCuMo-O and **e** corresponding diameter distribution of FeCoNiCuMo-O. **f**. XRD spectra of FeCoNiCuMo-O and CoNiCuMo-O. **g**. Representative TEM (insert pattern: selected area electron diffraction), **h** HRTEM image, **i** HAADF-STEM image, and the corresponding EDS mapping of FeCoNiCuMo-O.

from the combined interactions between neighboring atoms.[21] The synergistic interactions among elements in high entropy materials (HEMs) can regulate the electronic structure of the materials, resulting in their broader range for tuning binding energies and thereby optimizing the reaction process.[21−23] In addition, the inherent lattice distortion in HEMs also modifies the electron cloud distribution around the lattice oxygen, promoting its activation and achieving more efficient OER.[24,25] More importantly, the intrinsic enhancement of configurational entropy stabilizes HEMs, countering deleterious effects on crystal frameworks due to lattice oxygen involvement.[26] Among various fabrication techniques,[27−31] carbothermal shock (CTS) stands out for its operational simplicity, energy efficiency, and precision in compositional control.[22] The CTS provides rapid heating rates, which can effectively promote the homogeneous distribution of metal ions and facilitate the formation of high-entropy phases.[32] Fast cooling limits secondary or side reactions by reducing transient heating times and ensures uniform nanoparticle dispersion, thereby facilitating precise control over the reaction process.[33] Moreover, the rapid thermal cycling in air accelerates the oxidation process,[34] enabling the incorporation of oxygen into the high-entropy framework, which is essential for activating lattice oxygen in OER.

Fe, Co, Ni, Cu, and Mo are well-known transition metals that have been widely investigated for their role in OER. Fe, Co, and Ni with variable valence states facilitate electron transfer in the OER, lowering the energy barrier and accelerating kinetics.[35] Their unfilled *d* orbitals can hybridize with reactant orbitals, weakening bonds and promoting O−O bond formation.[36,37] In multimetallic systems, Cu is often included to improve electronic conductivity and facilitate electron transfer between active sites.[38] Previously, Mo was shown to influence charge redistribution and optimize adsorption of OER intermediates in high-entropy systems.[39] Inspired by the above, we prepared high-entropy oxides containing Fe, Co, Ni, Cu, and Mo (denoted as FeCoNiCuMo-O) by CTS. The CTS method ensures homogeneous blending of immiscible components, satisfying the high-entropy design. Notably, co-optimization of LOM and AEM is found to play a pivotal role in accelerating the reaction kinetics of FeCoNiCuMo-O, which is attributed to the optimization of the rate-determining step (RDS) for both mechanisms. Meanwhile, the augmented conformational entropy can bring about a remarkable prolongation of the catalyst stability. Consequently, FeCoNiCuMo-O exhibits exceptional electrocatalytic performance under alkaline conditions, with an overpotential (η_{10}) as low as 272 mV to reach 10 mA cm^{-2}, a Tafel slope of 41 mV dec^{-1}, and enduring electrolysis capacity spanning 240 h, markedly surpassing benchmarks set by RuO_2 (η_{10} = 313 mV, 97 mV dec^{-1}). Our study attempts to shed some light on the path forward for engineering economically viable OER electrocatalysts that excel in both efficiency and durability, hopefully representing a

https://doi.org/10.1021/acs.nanolett.4c05658
Nano Lett. XXXX, XXX, XXX−XXX

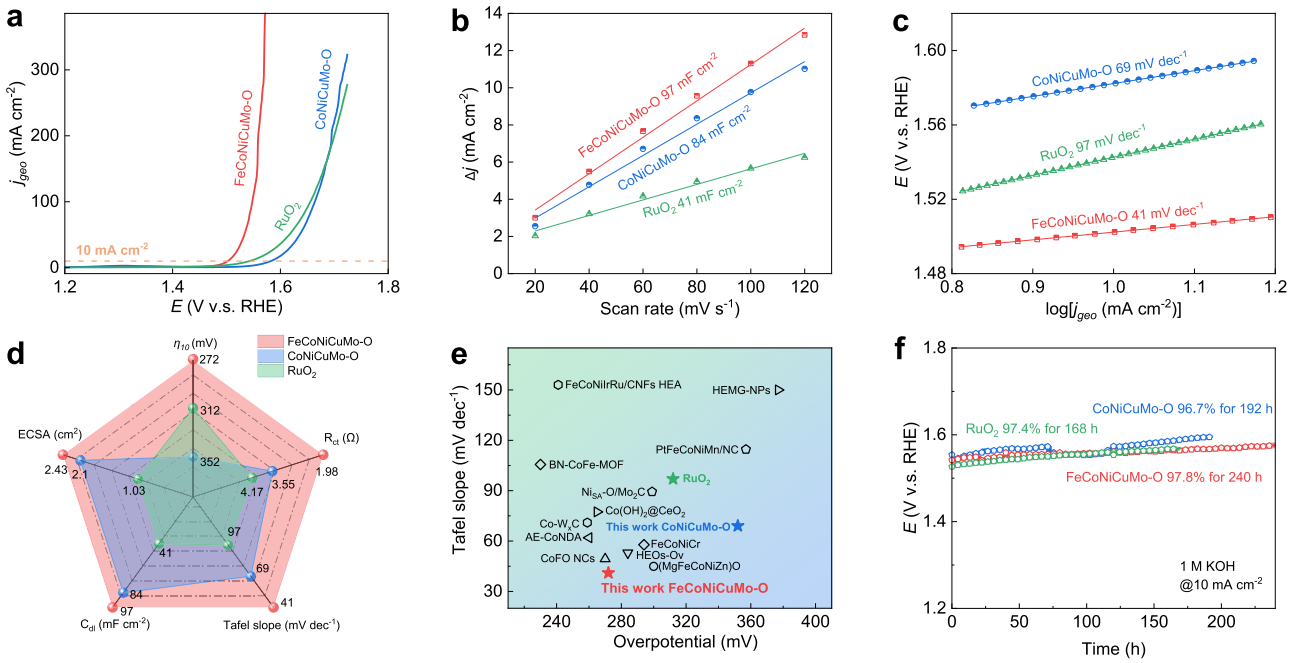

Figure 2. Electrochemical performance evaluation. **a**. LSV curves at a scan rate of 5 mV s^{-1}, **b** relationship between current density difference and scan rate (C_{dl} values calculated through linear fitting of the curves), **c** Tafel slopes, **d** OER performance comparison of FeCoNiCuMo-O, CoNiCuMo-O, and RuO_2. **e**. Comparison with the overpotential and Tafel slope of recently reported advanced OER catalysts. **f**. Stability tests at 10 mA cm^{-2} of FeCoNiCuMo-O, CoNiCuMo-O, and RuO_2.

meaningful step toward sustainable hydrogen production technologies.

Figure S1 shows the process for the preparation of FeCoNiCuMo-O and its comparative catalysts. A carbon cloth (CC) was first pretreated by CTS so as to improve its wettability (Figures S2 and S3). Good wettability of the substrate not only facilitates uniform distribution of the metal precursor solution to achieve homogeneous high-entropy mixing for the catalyst synthesis[22] but also increases reaction rates by enhancing charge transport and promoting ion diffusion during the OER process.[40] Then the CC was soaked in the metal precursor solution, dried, and processed by CTS again. Figure 1a illustrates the schematic of metal ions dispersing from the precursor solution to grow into nano crystalline particles. Figure 1b shows the temperature profile of CTS process with the characteristics of very short processing time in the second level and very high temperature close to 2000 K. The inset in Figure 1b shows the schematic of the CTS configuration and its photograph is shown in Figure 1c. Scanning electron microscopy (SEM) images in Figures 1d and S4 show dispersed FeCoNiCuMo-O particles on the CC fibers, with an average size of about 49 nm (Figure 1e). CoNiCuMo-O presents a similar morphology (Figure S5). The regular facets indicate the crystalline nature of the particles, which are confirmed by XRD spectra (Figure 1f). The diffraction peaks of both FeCoNiCuMo-O and CoNiCuMo-O exhibit a single hexagonal structure with the space group of *P*63/*mmc* (JCPDS #08-0384). Compared to standard diffraction peaks, a slight shift in some peaks of both samples indicates lattice distortion caused by multimetal mixing.[41,42] Transmission electron microscopy (TEM) further discloses the morphology of FeCoNiCuMo-O as nanocrystalline particles with regular edges (Figure 1g). High-resolution transmission electron microscopy (HRTEM) images reveal clear lattice fringes of FeCoNiCuMo-O, with a lattice spacing of 0.25 nm in the region marked by a red dashed line (Figure 1h). The selected area electron diffraction (SAED) pattern (inset in Figure 1h) again demonstrates the single-crystalline nature of the particle. High-angle annular dark-field scanning transmission electron microscopy (HAADF-STEM) and corresponding X-ray energy dispersive spectroscopy (EDS) mapping characterizations (Figure 1i) show the uniform distribution of Fe, Co, Ni, Cu, Mo, and O elements, indicating the successful synthesis of single-phase FeCoNiCuMo-O. Previous studies have demonstrated that ensuring a single-phase state is crucial for achieving atomic-level mixing of various elements, enabling synergistic properties that cannot be attained by individual components.[43] X-ray photoelectron spectroscopy (XPS) analysis shows that all metal elements are present in their oxidized states within the samples, as indicated by their binding energies compared to standard values for both metallic and oxidized forms (Figures S6−S10 and Tables S1 and S2).

A three-electrode system in 1 M KOH electrolyte solution was used to investigate the electrocatalytic performance of the synthesized catalysts during OER. In the performance testing, RuO_2 (SEM as shown in Figure S4c and d) is often selected as a comparison material because of its high catalytic activity, relatively high stability, and extensive research foundation, providing a reliable reference for the evaluation of catalysts. As illustrated in Figure 2a, the overpotential (η) required for FeCoNiCuMo-O to reach the geometric area normalized current densities (j_{geo}) of 10, 50, 100, and 200 mA/cm^2 are 272, 303, 317, and 328 mV, respectively, much lower than those for CoNiCuMo-O (352, 406, 433, and 464 mV) and RuO_2 (312, 386, 425, and 470 mV). This demonstrates a substantial enhancement in the apparent electrocatalytic activity of FeCoNiCuMo-O. The intrinsic activity of the catalysts can be reflected by normalizing the current with electrochemically active surface area (ECSA), which is associated with the double-layer capacitance (C_{dl}). According

https://doi.org/10.1021/acs.nanolett.4c05658
Nano Lett. XXXX, XXX, XXX−XXX

Scheme 1. Schematic Diagram of AEM and LOM

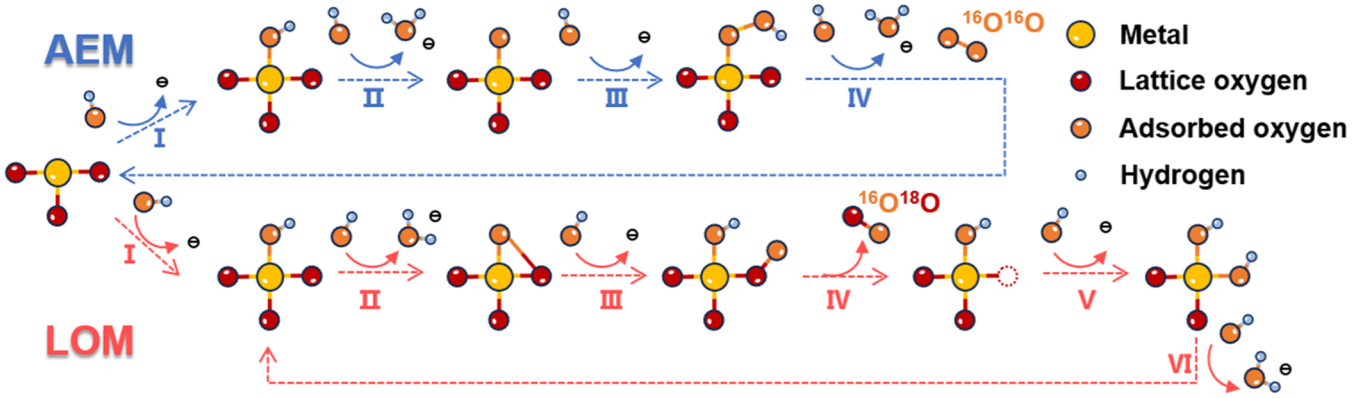

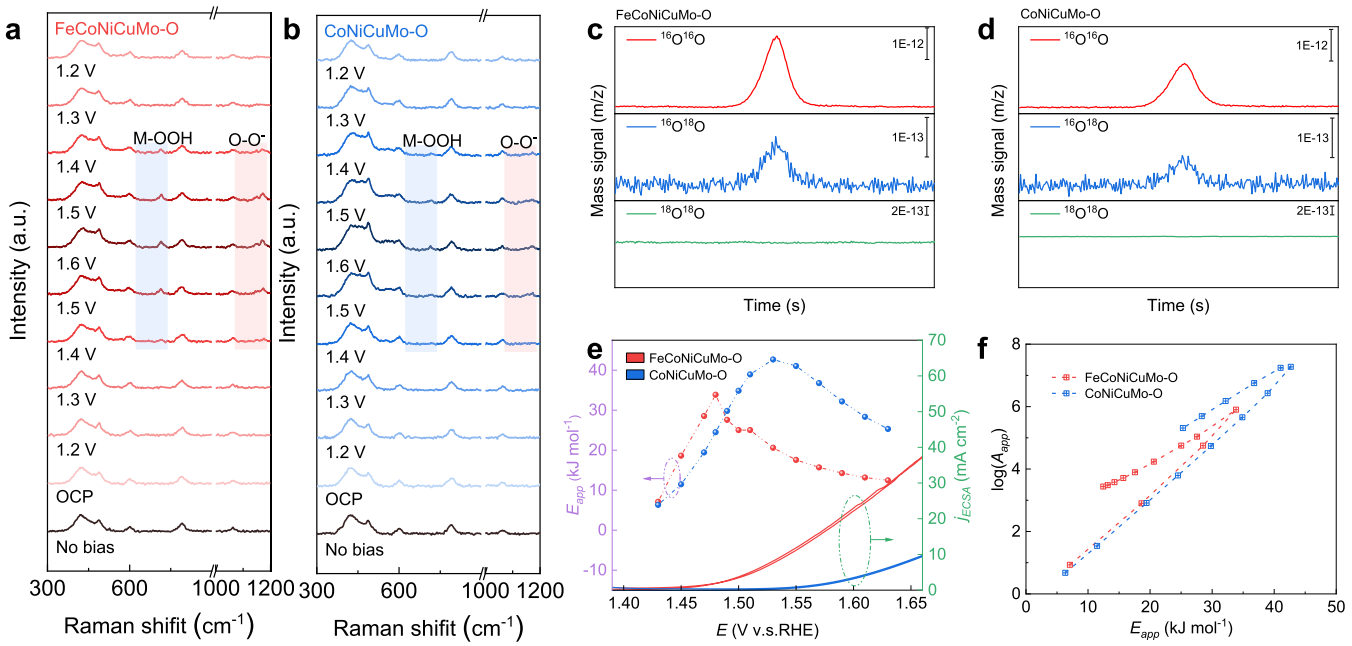

Figure 3. *In situ* Raman spectra of **a** FeCoNiCuMo-O and **b** CoNiCuMo-O. DEMS signals of $^{16}O^{16}O$, $^{16}O^{18}O$, and $^{18}O^{18}O$ from the gaseous products for ^{18}O-labeled **c** FeCoNiCuMo-O and **d** CoNiCuMo-O. **e.** The E_{app} values (purple *Y*-axis) were derived from CV curves performed at various temperatures, as detailed in Figures S19−S21 in the Supporting Information. CV curves were collected at 20 °C (green *Y*-axis). **f.** The logarithm of the A_{app} for both FeCoNiCuMo-O and CoNiCuMo-O was calculated at fixed potentials, based on the intercepts found in the Arrhenius plots shown in Figures S19 and S21.

to the C_{dl} values (Figures 2b and S11), the ECSA is calculated as 2.43 (FeCoNiCuMo-O), 2.10 (CoNiCuMo-O), and 1.03 (RuO_2) cm^2, respectively, indicating that FeCoNiCuMo-O has the most active sites as well. The ECSA-normalized LSV curves show that the intrinsic activity of FeCoNiCuMo-O remains superior to the other two (Figure S12).

The Tafel plot, extrapolated from the polarization curves and depicted in Figure 2c, elucidates the kinetics underlying the OER process. The Tafel slope of 41 mV dec^{-1} for FeCoNiCuMo-O is much lower than that of CoNiCuMo-O (69 mV dec^{-1}) and RuO_2 (97 mV dec^{-1}). The improved catalytic reaction in FeCoNiCuMo-O is also evidenced by its notably lower charge transfer resistance than those of CoNiCuMo-O and RuO_2 (Figure S13). Figure 2d summarizes the comparison of OER performance of FeCoNiCuMo-O, CoNiCuMo-O, and RuO_2, showing that FeCoNiCuMo-O is superior in all aspects to the other two. The comparison with the literature further shows the superior performance of our designed catalysts in the aspect of the lower overpotential and Tafel slope of FeCoNiCuMo-O (Figure 2e and Table S4).

To elucidate whether the enhanced performance is induced by the increased entropy due to the construction of multiple elements, since it has been reported that high entropy materials are designed for high-efficiency catalysts,[38] other catalysts with four out of the five metals have also been investigated (Figures S14−S16). All catalysts containing Fe show similar reaction kinetics, close to that of FeCoNiCuMo-O, confirming the efficiency improvement is induced by Fe but not entropy increase.

However, the enhanced configurational entropy can ensure robust structural integrity during prolonged electrolysis processes.[44] In the realm of OER catalysts utilized in basic environments, a predominant challenge is their inadequate stability, which precludes the use of many catalysts.[45] Contrary to these limitations, FeCoNiCuMo-O demonstrates remarkable durability, exhibiting a robust performance during a 240-h continuous chronopotentiometry (CP) test at 10 mA cm^{-2},

https://doi.org/10.1021/acs.nanolett.4c05658
Nano Lett. XXXX, XXX, XXX−XXX

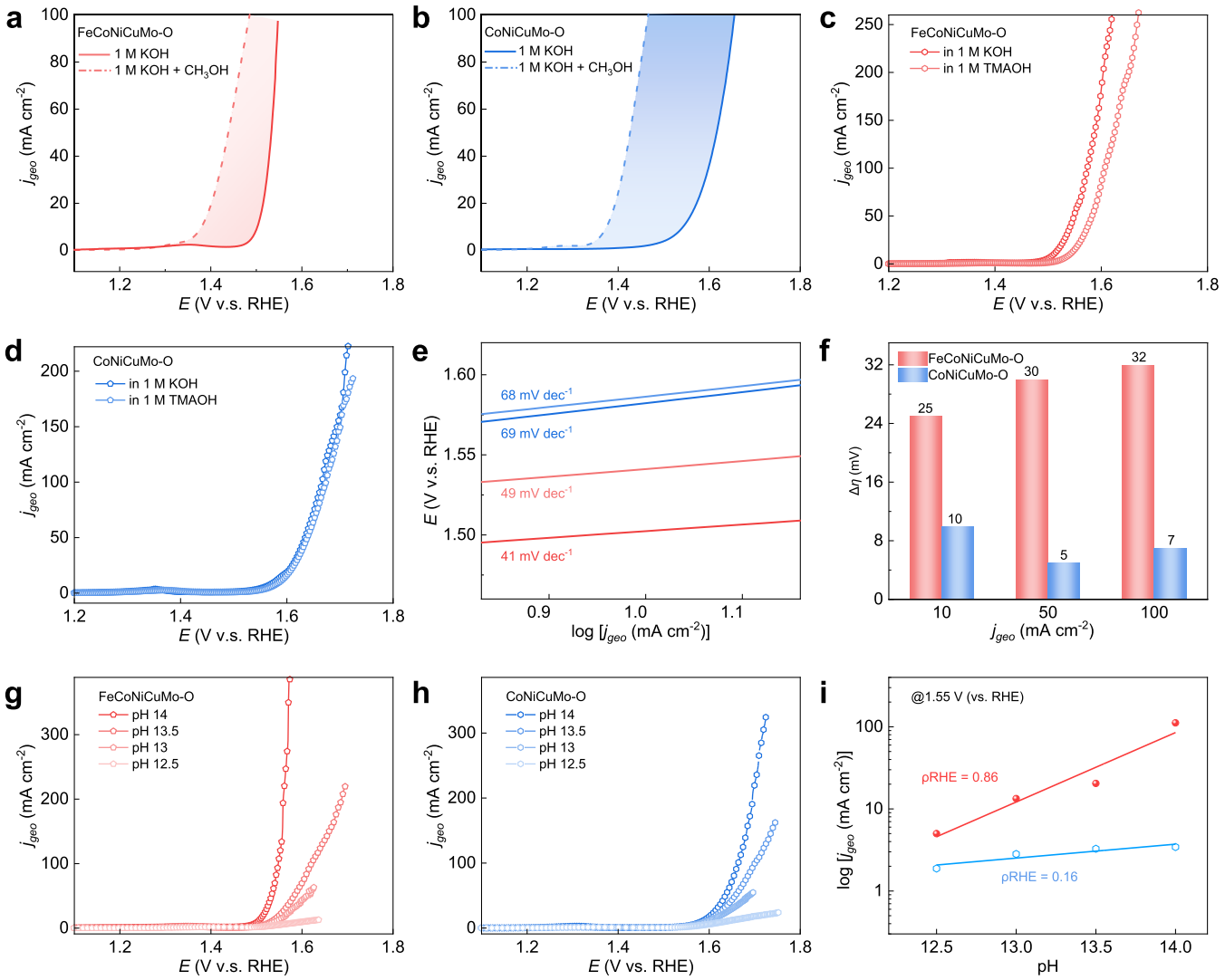

Figure 4. LSV curves of **a** FeCoNiCuMo-O, and **b** CoNiCuMo-O in 1 M KOH (with and without 0.602 M methanol). LSV curves in 1 M KOH and 1 M TMAOH of **c** FeCoNiCuMo-O and **d** CoNiCuMo-O, shift of **e** Tafel slope and **f** $\Delta\eta$. LSV curves were recorded in 1 M KOH at pH values of 12.5, 13, 13.5, and 14 of **g** FeCoNiCuMo-O and **h** CoNiCuMo-O. **i** The j at 1.55 V (v.s. RHE) is plotted on a logarithmic scale as a function of pH, from which the ρ^{RHE} is derived.

with the voltage decaying by only 2.2%, much stable than CoNiCuMo-O (3.3% for 192 h) and RuO_2 (2.6% for 168 h) (Figure 2f), and other Fe-containing four-metal-element catalysts as well (Figure S17). It exhibits commendable long-term stability even under a higher current density of 50 mA cm^{-2} (Figure S18).

The superior performance of FeCoNiCuMo-O can be explained with both AEM and LOM. Scheme 1 schematically shows the two mechanisms. AEM is normally thought to involve four simultaneous proton−electron transfer (CPET) reactions.[25] Specifically, OH^- in solution is first adsorbed on the surface of the catalyst (step I) and subsequently deprotonated to form *O (step II). This is followed by the combination of another OH^- to form *OOH (O−O bond formation) (step III), and finally O_2 is precipitated along with the deprotonation of *OOH (step IV). There exists a linear free energy relationship (LFER) between *OH and *OOH, with ΔG_{*OOH}-ΔG_{*OH} = 3.2 ± 0.2 eV. Although optimizing the adsorption of *OH generally leads to a corresponding improvement in the adsorption of *OOH, the constant energy difference limits the potential for achieving optimal performance across all reaction steps. On the other hand, the LOM process involves direct coupling of *O with lattice oxygen (step II) and subsequent adsorption of OH^- to form *OO and *OH intermediates (step III). This intermediate releases O_2 and generates oxygen vacancies (O_{vs}) (step IV), followed by deprotonation (step VI) to restore the initial surface after OH^- fills the O_{vs} to form *OH (step V).[12] Lattice oxygen is involved in direct O−O coupling, bypassing the LFER limitation and thus providing a faster reaction path.

The involvement of AEM and LOM can be directly identified by the *in situ* Raman spectroscopy electrochemical analysis, as shown in Figure 3a and b. Initially, the Raman spectra of both FeCoNiCuMo-O and CoNiCuMo-O, taken before immersion in the electrolyte and at open circuit potential (OCP), are virtually identical, confirming that the laser does not substantially alter the materials. No new peaks emerge in the Raman spectra of either sample until the voltage reaches 1.4 V (v.s. RHE). As the voltage is progressively increased from 1.4 to 1.6 V (v.s. RHE), a distinct band appears at ∼566 cm^{-1}, where FeCoNiCuMo-O and CoNiCuMo-O exhibit apparent peak intensity, corresponding to the lattice

https://doi.org/10.1021/acs.nanolett.4c05658
Nano Lett. XXXX, XXX, XXX−XXX

translation mode of M-OOH.[46−48] Then, this peak gradually diminishes as the voltage is lowered from 1.6 back to 1.4 V (v.s. RHE). Clearly, FeCoNiCuMo-O has a stronger M-OOH characteristic peak than CoNiCuMo-O. Simultaneously, within the same voltage range, the appearance and disappearance of the $O-O^-$ characteristic peak at ∼1170 cm^{-1} align with those of the M-OOH feature.[49,50] The more pronounced M-OOH and $O-O^-$ peaks in FeCoNiCuMo-O indicate its superior OER performance is due to the enhanced contributions of both AEM and LOM. ^{18}O-labeled *in situ* differential electrochemical mass spectrometry (DEMS) further tests the synergistic enhancement of AEM and LOM in FeCoNiCuMo-O. Initially, both catalysts were activated five times in a 1 M KOH solution using $H_2{}^{18}O$ as the solvent to label the catalyst surface, followed by LSV tests in an electrolyte using $H_2{}^{16}O$ as the solvent. The dynamic surface reconstruction facilitates the incorporation of heavy oxygen isotopes (^{18}O) into the lattice structure. Figure 3c and d shows the signals of the products during the testing process. Both samples displayed signals from $^{16}O^{18}O$ products labeled with ^{18}O, which gradually decreased in intensity with an increasing number of tests, indicating the consumption of the labeled ^{18}O isotope. These observations confirm the involvement of lattice oxygen in the reactions for both FeCoNiCuMo-O and CoNiCuMo-O. Notably, the intensity of the $^{16}O^{16}O$ and $^{16}O^{18}O$ signal peaks in FeCoNiCuMo-O was higher than in CoNiCuMo-O, indicating its higher efficiency according to both mechanisms, which is consistent with the *in situ* Raman spectroscopy analysis.

To link the reaction energetics with the underlying mechanistic pathways, temperature-dependent kinetic analyses of FeCoNiCuMo-O and CoNiCuMo-O electrocatalysts were carried out in the range of 20−70 °C (Figures S19−S21), and the apparent activation energy (E_{app}) and pre-exponential factor (A_{app})[51] were extracted according to Arrhenius equation (see the Supporting Information section for specific calculations).[52] To comprehensively capture the variation of E_{app} with potential, the analyses were performed below and above the catalytic onset potential. The E_{app} values of both catalysts peaked near their respective catalytic OER onset potentials (Figure 3e), which is consistent with the observation that FeCoNiCuMo-O requires a lower overpotential than CoNiCuMo-O to effectively catalyze OER. The lower E_{app} value in FeCoNiCuMo-O indicates reduces in the energy barrier and kinetic constraints associated with the RDS for intermediate formation.[52] This can be attributed to the emergence of new pathways mediated by lattice oxygen and the optimization of active sites in the AEM.

A_{app} is positively correlated with the number of active intermediates and the concentration of active sites in the rate-determining step.[53] However, FeCoNiCuMo-O exhibits faster reaction kinetics despite its lower A_{app} (Figure 3f), suggesting a reduced reliance on these factors. This implies that lattice oxygen provides an alternative reaction pathway, reducing the need for surface active sites and emphasizing the more pivotal role of LOM in enhancing OER activity.[54]

The surface differences in terms of active sites in FeCoNiCuMo-O and CoNiCuMo-O can be partially explained by the distinct binding energy shifts observed for the constituent elements (Figure S7). These variations significantly influence the activity of the active sites, leading to changes in their interaction energy with reaction intermediates, ultimately resulting in different kinetic behaviors, such as reactivity and selectivity.[55]

The enhancement of AEM for FeCoNiCuMo-O can be explained according to the LSV curves of FeCoNiCuMo-O and CoNiCuMo-O in both CH_3OH-free and CH_3OH-containing electrolytes, as shown in Figure 4, panels a and b, respectively. Methanol is known to compete with the electrocatalyst surface for the adsorption of *OH intermediates.[39,55] The smaller current density difference observed for FeCoNiCuMo-O compared to CoNiCuMo-O suggests a weaker *OH adsorption capacity for FeCoNiCuMo-O. This is further corroborated by the increased intensity of the M-O peak in the O 1s XPS spectrum of FeCoNiCuMo-O, which indicates a greater ease of *OH dissociation (Figure S7 and Table S1). The above results clarify that the enhanced M-OOH peak observed in the *in situ* Raman spectra is due to the weakened *OH adsorption on the FeCoNiCuMo-O surface, which promotes the accumulation of M-OOH species. This, in turn, optimizes the RDS of the AEM pathway.[56]

Similarly, tetramethylammonium hydroxide (TMAOH) is commonly used as a chemical probe to detect active oxygen species ($O_2{}^{2-}$) formed during deprotonation in the LOM process, as the strong electrostatic interaction between TMA^+ and the $O_2{}^{2-}$ negatively impacts the activity of LOM-based electrocatalysts. When comparing data collected in 1 M KOH and TMAOH electrolytes (Figure 4c and d), the differences in Tafel slopes (Figure 4e) and overpotentials at various current densities (Figure 4f) are significantly greater for FeCoNiCuMo-O than for CoNiCuMo-O. The OER activity of FeCoNiCuMo-O is significantly inhibited in TMAOH, which indicates that the deprotonation step in LOM is strongly interfered with by TMA^+. It can be inferred that the RDS in FeCoNiCuMo-O has been optimized, thereby enhancing the contribution of LOM to OER.[25,57] To further investigate the reasons behind the enhancement of lattice oxygen in FeCoNiCuMo-O, LSV tests were performed in electrolytes with varying pH values. As mentioned above, the RDS of LOM solely involves proton transfer, which contributes to its pronounced pH dependence.[58−60] As shown in Figure 4g and h, the OER activity of FeCoNiCuMo-O significantly improved with increasing pH, while CoNiCuMo-O demonstrated only a slight pH dependency. Simultaneously, the order of the proton reaction was calculated on the reversible hydrogen electrode (RHE) scale (ρ^{RHE}) to assess the dependency of reaction kinetics on proton activity, providing deeper insight into effect of pH on activity.[61] A parameter closer to 1 indicates a higher sensitivity of the catalyst to pH changes.[62] The ρ^{RHE} of CoNiCuMo-O was 0.16, significantly lower than that of FeCoNiCuMo-O at 0.86 (Figure 4i). This suggests that the optimization of the LOM pathway for FeCoNiCuMo-O was achieved by increasing the proton transfer kinetics at the catalyst surface. Thus, FeCoNiCuMo-O exhibits faster kinetics and stronger LOM than CoNiCuMo-O. It has been reported that Fe can improve metal−oxygen covalency and thus lattice oxygen activation, which makes catalysts more inclined to follow the LOM.[35] In addition, a series of literature reports that the introduction of Fe significantly improves the chemisorption of intermediates for both AEM and LOM.[55,63] However, much is still unknown in this regard, and more in-depth studies could be carried out in the future.

In summary, the synthesis of FeCoNiCuMo-O electrocatalyst via a CTS strategy leverages the advantages of this

https://doi.org/10.1021/acs.nanolett.4c05658
Nano Lett. XXXX, XXX, XXX−XXX

method for fabricating high-entropy materials. *In-situ* Raman and DEMS revealed that the OER on FeCoNiCuMo-O was performed by both LOM and AEM. Further, kinetic and extensive chemical probe tests confirmed the optimization of intermediate *OH adsorption in AEM and proton transfer in LOM. This dual pathway optimization allowed FeCoNiCuMo-O to overcome the overpotential limitations imposed by LFER. In addition, the high entropy design ensures the stability of FeCoNiCuMo-O during prolonged electrolysis. This work endeavor furnishes invaluable inspiration for the rational design of highly stable and catalytically active non-noble metal catalysts.

■ ASSOCIATED CONTENT

Supporting Information

The Supporting Information is available free of charge at https://pubs.acs.org/doi/10.1021/acs.nanolett.4c05658.

Experimental methods, illustration of the process for preparing FeCoNiCuMo-O, temperature profile of raw CC during the CTS process, contact angle test for processed CC and raw CC, the characterizations of a series of samples (SEM, XPS, XRD), and electrochemical data (PDF)

■ AUTHOR INFORMATION

Corresponding Authors

Fangzhu Qing − *Shenzhen Institute for Advanced Study, University of Electronic Science and Technology of China, Shenzhen 518110, China; School of Integrated Circuit Science and Engineering (Exemplary School of Microelectronics) and State Key Laboratory of Electronic Thin Films and Integrated Devices, University of Electronic Science and Technology of China, Chengdu 611731, China*; Email: qingfz@uestc.edu.cn

Yuanfu Chen − *School of Integrated Circuit Science and Engineering (Exemplary School of Microelectronics) and State Key Laboratory of Electronic Thin Films and Integrated Devices, University of Electronic Science and Technology of China, Chengdu 611731, China*; orcid.org/0000-0002-6561-1684; Email: yfchen@uestc.edu.cn

Xuesong Li − *Shenzhen Institute for Advanced Study, University of Electronic Science and Technology of China, Shenzhen 518110, China; School of Integrated Circuit Science and Engineering (Exemplary School of Microelectronics) and State Key Laboratory of Electronic Thin Films and Integrated Devices, University of Electronic Science and Technology of China, Chengdu 611731, China*; orcid.org/0000-0002-1157-0266; Email: lxs@uestc.edu.cn

Authors

Wanyi Liao − *Shenzhen Institute for Advanced Study, University of Electronic Science and Technology of China, Shenzhen 518110, China*

Qian Liu − *Shenzhen Institute for Advanced Study, University of Electronic Science and Technology of China, Shenzhen 518110, China*

Rongxuan Wu − *Shenzhen Institute for Advanced Study, University of Electronic Science and Technology of China, Shenzhen 518110, China*

Congli Zhou − *School of Integrated Circuit Science and Engineering (Exemplary School of Microelectronics) and State Key Laboratory of Electronic Thin Films and Integrated Devices, University of Electronic Science and Technology of China, Chengdu 611731, China*

Lina Chen − *Shenzhen Institute for Advanced Study, University of Electronic Science and Technology of China, Shenzhen 518110, China*

Complete contact information is available at: https://pubs.acs.org/10.1021/acs.nanolett.4c05658

Notes

The authors declare no competing financial interest.

■ ACKNOWLEDGMENTS

This work was supported by the Shenzhen Science and Technology Program (No. KQTD20200820113010022)

■ REFERENCES

(1) Chen, F.-Y.; Wu, Z.-Y.; Adler, Z.; Wang, H. Stability Challenges of Electrocatalytic Oxygen Evolution Reaction: From Mechanistic Understanding to Reactor Design. *Joule* **2021**, *5* (7), 1704−1731.

(2) Seh, Z. W.; Kibsgaard, J.; Dickens, C. F.; Chorkendorff, I.; Nørskov, J. K.; Jaramillo, T. F. Combining Theory and Experiment in Electrocatalysis: Insights into Materials Design. *Science* **2017**, *355* (6321), No. eaad4998.

(3) Zou, X.; Zhang, Y. Noble Metal-Free Hydrogen Evolution Catalysts for Water Splitting. *Chem. Soc. Rev.* **2015**, *44* (15), 5148−5180.

(4) Lin, C.; Li, J.-L.; Li, X.; Yang, S.; Luo, W.; Zhang, Y.; Kim, S.-H.; Kim, D.-H.; Shinde, S. S.; Li, Y.-F.; et al. In-Situ Reconstructed Ru Atom Array on α-MnO_2 with Enhanced Performance for Acidic Water Oxidation. *Nat. Catal.* **2021**, *4* (12), 1012−1023.

(5) Bergmann, A.; Jones, T. E.; Martinez Moreno, E.; Teschner, D.; Chernev, P.; Gliech, M.; Reier, T.; Dau, H.; Strasser, P. Unified Structural Motifs of the Catalytically Active State of Co(oxyhydr)-oxides during the Electrochemical Oxygen Evolution Reaction. *Nat. Catal.* **2018**, *1* (9), 711−719.

(6) Wu, Y.; Zhao, Y.; Zhai, P.; Wang, C.; Gao, J.; Sun, L.; Hou, J. Triggering Lattice Oxygen Activation of Single-Atomic Mo Sites Anchored on Ni−Fe Oxyhydroxides Nanoarrays for Electrochemical Water Oxidation. *Adv. Mater.* **2022**, *34* (29), 2202523.

(7) Du, L.; Xing, L.; Zhang, G.; Dubois, M.; Sun, S. Strategies for Engineering High-Performance PGM-Free Catalysts toward Oxygen Reduction and Evolution Reactions. *Small Methods* **2020**, *4* (6), 2000016.

(8) Suntivich, J.; May, K. J.; Gasteiger, H. A.; Goodenough, J. B.; Shao-Horn, Y. A Perovskite Oxide Optimized for Oxygen Evolution Catalysis from Molecular Orbital Principles. *Science* **2011**, *334* (6061), 1383−1385.

(9) Wu, T.; Sun, S.; Song, J.; Xi, S.; Du, Y.; Chen, B.; Sasangka, W. A.; Liao, H.; Gan, C. L.; Scherer, G. G.; et al. Iron-Facilitated Dynamic Active-Site Generation on Spinel CoAl2O4 with Self-Termination of Surface Reconstruction For Water Oxidation. *Nat. Catal.* **2019**, *2* (9), 763−772.

(10) Song, J.; Wei, C.; Huang, Z.-F.; Liu, C.; Zeng, L.; Wang, X.; Xu, Z. J. A Review on Fundamentals for Designing Oxygen Evolution Electrocatalysts. *Chem. Soc. Rev.* **2020**, *49* (7), 2196−2214.

(11) Xiao, K.; Wang, Y.; Wu, P.; Hou, L.; Liu, Z.-Q. Activating Lattice Oxygen in Spinel $ZnCo_2O_4$ through Filling Oxygen Vacancies with Fluorine for Electrocatalytic Oxygen Evolution. *Angew. Chem., Int. Ed.* **2023**, *62* (24), No. e202301408.

(12) Huang, Z.-F.; Song, J.; Du, Y.; Xi, S.; Dou, S.; Nsanzimana, J. M. V.; Wang, C.; Xu, Z. J.; Wang, X. Chemical and Structural Origin of Lattice Oxygen Oxidation in Co−Zn Oxyhydroxide Oxygen Evolution Electrocatalysts. *Nat. Energy* **2019**, *4* (4), 329−338.

(13) Song, K.; Zhang, H.; Lin, Z.; Wang, Z.; Zhang, L.; Shi, X.; Shen, S.; Chen, S.; Zhong, W. Interfacial Engineering of Cobalt Thiophosphate with Strain Effect and Modulated Electron Structure

for Boosting Electrocatalytic Hydrogen Evolution Reaction. *Adv. Funct. Mater.* **2024**, *34* (12), 2312672.
(14) Vojvodic, A.; Nørskov, J. K. Optimizing Perovskites for the Water-Splitting Reaction. *Science* **2011**, *334* (6061), 1355−1356.
(15) Huang, Z.-F.; Wang, J.; Peng, Y.; Jung, C.-Y.; Fisher, A.; Wang, X. Design of Efficient Bifunctional Oxygen Reduction/Evolution Electrocatalyst: Recent Advances and Perspectives. *Adv. Energy Mater.* **2017**, *7* (23), 1700544.
(16) Rong, X.; Parolin, J.; Kolpak, A. M. A Fundamental Relationship between Reaction Mechanism and Stability in Metal Oxide Catalysts for Oxygen Evolution. *ACS Catal.* **2016**, *6* (2), 1153−1158.
(17) Grimaud, A.; Hong, W. T.; Shao-Horn, Y.; Tarascon, J. M. Anionic Redox Processes for Electrochemical Devices. *Nat. Mater.* **2016**, *15* (2), 121−126.
(18) Ren, X.; Zhai, Y.; Yang, N.; Wang, B.; Liu, S. Lattice Oxygen Redox Mechanisms in the Alkaline Oxygen Evolution Reaction. *Adv. Funct. Mater.* **2024**, *34* (32), 2401610.
(19) Lin, C.; Li, J.-L.; Li, X.; Yang, S.; Luo, W.; Zhang, Y.; Kim, S.-H.; Kim, D.-H.; Shinde, S. S.; Li, Y.-F.; et al. In-Situ Reconstructed Ru Atom Array on α-MnO_2 with Enhanced Performance for Acidic Water Oxidation. *Nat. Catal.* **2021**, *4* (12), 1012−1023.
(20) Shi, Z.; Wang, Y.; Li, J.; Wang, X.; Wang, Y.; Li, Y.; Xu, W.; Jiang, Z.; Liu, C.; Xing, W.; et al. Confined Ir Single Sites with Triggered Lattice Oxygen Redox: Toward Boosted and Sustained Water Oxidation Catalysis. *Joule* **2021**, *5* (8), 2164−2176.
(21) Löffler, T.; Ludwig, A.; Rossmeisl, J.; Schuhmann, W. What Makes High-Entropy Alloys Exceptional Electrocatalysts? *Angew. Chem., Int. Ed.* **2021**, *60* (52), 26894−26903.
(22) Yao, Y.; Huang, Z.; Xie, P.; Lacey, S. D.; Jacob, R. J.; Xie, H.; Chen, F.; Nie, A.; Pu, T.; Rehwoldt, M.; et al. Carbothermal Shock Synthesis of High-Entropy-Alloy Nanoparticles. *Science* **2018**, *359* (6383), 1489−1494.
(23) Batchelor, T. A. A.; Pedersen, J. K.; Winther, S. H.; Castelli, I. E.; Jacobsen, K. W.; Rossmeisl, J. High-Entropy Alloys as a Discovery Platform for Electrocatalysis. *Joule* **2019**, *3* (3), 834−845.
(24) Porokhin, S. V.; Nikitina, V. A.; Aksyonov, D. A.; Filimonov, D. S.; Pazhetnov, E. M.; Mikheev, I. V.; Abakumov, A. M. Mixed-Cation Perovskite $La_{0.6}Ca_{0.4}Fe_{0.7}Ni_{0.3}O_{2.9}$ as a Stable and Efficient Catalyst for the Oxygen Evolution Reaction. *ACS Catal.* **2021**, *11* (13), 8338−8348.
(25) Zhang, N.; Chai, Y. Lattice Oxygen Redox Chemistry in solid-state electrocatalysts for Water Oxidation. *Energy Environ. Sci.* **2021**, *14* (9), 4647−4671.
(26) Pan, Y.; Xu, X.; Zhong, Y.; Ge, L.; Chen, Y.; Veder, J.-P. M.; Guan, D.; O'Hayre, R.; Li, M.; Wang, G.; Wang, H.; Zhou, W.; Shao, Z. Direct Evidence of Boosted Oxygen Evolution over Perovskite by Enhanced Lattice Oxygen Participation. *Nat. Commun.* **2020**, *11* (1), 2002.
(27) Huang, K.; Xia, J.; Lu, Y.; Zhang, B.; Shi, W.; Cao, X.; Zhang, X.; Woods, L. M.; Han, C.; Chen, C.; Wang, T.; Wu, J.; Huang, Y. Self-Reconstructed Spinel Surface Structure Enabling the Long-Term Stable Hydrogen Evolution Reaction/Oxygen Evolution Reaction Efficiency of FeCoNiRu High-Entropy Alloyed Electrocatalyst. *Adv. Sci.* **2023**, *10* (14), 2300094.
(28) Li, K.; Chen, W. Recent Progress in High-Entropy Alloys for Catalysts: Synthesis, Applications, and Prospects. *Mater. Today Energy* **2021**, *20*, 100638.
(29) Bondesgaard, M.; Broge, N. L. N.; Mamakhel, A.; Bremholm, M.; Iversen, B. B. General Solvothermal Synthesis Method for Complete Solubility Range Bimetallic and High-Entropy Alloy Nanocatalysts. *Adv. Funct. Mater.* **2019**, *29* (50), 1905933.
(30) Liu, M.; Zhang, Z.; Okejiri, F.; Yang, S.; Zhou, S.; Dai, S. Entropy-Maximized Synthesis of Multimetallic Nanoparticle Catalysts via a Ultrasonication-Assisted Wet Chemistry Method under Ambient Conditions. *Adv. Mater. Interfaces* **2019**, *6* (7), 1900015.
(31) Liu, Y. C.; Tian, X. L.; Han, Y. C.; Chen, Y. A.; Hu, W. B. High-Temperature Shock Synthesis of High-Entropy-Alloy Nanoparticles for Catalysis. *Chin. J. Catal.* **2023**, *48*, 66−89.
(32) Chen, F.; Yao, Y.; Nie, A.; Xu, S.; Dai, J.; Hitz, E.; Li, Y.; Lu, A.; Huang, Z.; Li, T.; Shahbazian-Yassar, R.; Hu, L. High-Temperature Atomic Mixing toward Well-Dispersed Bimetallic Electrocatalysts. *Adv. Energy Mater.* **2018**, *8* (25), 1800466.
(33) Dong, Q.; Hu, S.; Hu, L. Electrothermal Synthesis of Commodity Chemicals. *Nat. Chem. Eng.* **2024**, *1* (11), 680−690.
(34) Li, T.; Yao, Y.; Huang, Z.; Xie, P.; Liu, Z.; Yang, M.; Gao, J.; Zeng, K.; Brozena, A. H.; Pastel, G.; et al. Denary Oxide Nanoparticles as Highly Stable Catalysts for Methane Combustion. *Nat. Catal.* **2021**, *4* (1), 62−70.
(35) Ye, P.; Fang, K.; Wang, H.; Wang, Y.; Huang, H.; Mo, C.; Ning, J.; Hu, Y. Lattice Oxygen Activation and Local Electric Field Enhancement by Co-Doping Fe and F in CoO Nanoneedle Arrays for Industrial Electrocatalytic Water Oxidation. *Nat. Commun.* **2024**, *15* (1), 1012.
(36) He, R.; Yang, L.; Zhang, Y.; Jiang, D.; Lee, S.; Horta, S.; Liang, Z.; Lu, X.; Ostovari Moghaddam, A.; Li, J.; Ibanez, M.; Xu, Y.; Zhou, Y.; Cabot, A. A 3d-4d-5d High Entropy Alloy as a Bifunctional Oxygen Catalyst for Robust Aqueous Zinc−Air Batteries. *Adv. Mater.* **2023**, *35* (46), 2303719.
(37) Wang, Z.; Shen, S.; Wang, J.; Zhong, W. Modulating the D-Band Center of Electrocatalysts for Enhanced Water Splitting. *Chem.—Eur. J.* **2024**, *30* (70), No. e202402725.
(38) Zhu, H.; Sun, S.; Hao, J.; Zhuang, Z.; Zhang, S.; Wang, T.; Kang, Q.; Lu, S.; Wang, X.; Lai, F.; et al. A High-Entropy Atomic Environment Converts Inactive to Active Sites for Electrocatalysis. *Energy Environ. Sci.* **2023**, *16* (2), 619−628.
(39) Mei, Y.; Feng, Y.; Zhang, C.; Zhang, Y.; Qi, Q.; Hu, J. High-Entropy Alloy with Mo-Coordination as Efficient Electrocatalyst for Oxygen Evolution Reaction. *ACS Catal.* **2022**, *12* (17), 10808−10817.
(40) Liu, Z.; Zhao, Z.; Wang, Y.; Dou, S.; Yan, D.; Liu, D.; Xia, Z.; Wang, S. In Situ Exfoliated, Edge-Rich, Oxygen-Functionalized Graphene from Carbon Fibers for Oxygen Electrocatalysis. *Adv. Mater.* **2017**, *29* (18), 1606207.
(41) Zeng, K.; Zhang, J.; Gao, W.; Wu, L.; Liu, H.; Gao, J.; Li, Z.; Zhou, J.; Li, T.; Liang, Z.; Xu, B.; Yao, Y. Surface-Decorated High-Entropy Alloy Catalysts with Significantly Boosted Activity and Stability. *Adv. Funct. Mater.* **2022**, *32* (33), 2204643.
(42) Chang, X.; Zeng, M.; Liu, K.; Fu, L. Phase Engineering of High-Entropy Alloys. *Adv. Mater.* **2020**, *32* (14), 1907226.
(43) Sun, Y.; Dai, S. High-Entropy Materials for Catalysis: A New Frontier. *Science. Sci. Adv.* **2021**, *7* (20), No. eabg1600.
(44) Jo, S.; Kim, M.-C.; Lee, K. B.; Choi, H.; Zhang, L.; Sohn, J. I. Nonprecious High-Entropy Chalcogenide Glasses-Based Electrocatalysts for Efficient and Stable Acidic Oxygen Evolution Reaction in Proton Exchange Membrane Water Electrolysis. *Adv. Energy Mater.* **2023**, *13* (35), 2301420.
(45) Cong, W.; Dong, W.; Yan, Y.; Cao, X.; Xu, Y.; Liu, Z.; Liu, J.; Yang, J.; Liu, X.; Yang, Y.; Fu, L.; Wang, M.; Zhang, T.; Zhou, J. Adjacent-Confined Pyrolysis for High-Density Phase Boundaries in Mo_2C Nanosheets to Boost Oxygen Evolution. *Adv. Funct. Mater.* **2024**, *34* (36), 2401990.
(46) Konkena, B.; Masa, J.; Botz, A. J. R.; Sinev, I.; Xia, W.; Koßmann, J.; Drautz, R.; Muhler, M.; Schuhmann, W. Metallic $NiPS_3$@NiOOH Core−Shell Heterostructures as Highly Efficient and Stable Electrocatalyst for the Oxygen Evolution Reaction. *ACS Catal.* **2017**, *7* (1), 229−237.
(47) Deabate, S.; Fourgeot, F.; Henn, F. X-Ray Diffraction and Micro-Raman Spectroscopy Analysis of New Nickel Hydroxide Obtained by Electrodialysis. *J. Power Sources* **2000**, *87* (1), 125−136.
(48) Bantignies, J. L.; Deabate, S.; Righi, A.; Rols, S.; Hermet, P.; Sauvajol, J. L.; Henn, F. New Insight into the Vibrational Behavior of Nickel Hydroxide and Oxyhydroxide Using Inelastic Neutron Scattering, Far/Mid-Infrared and Raman Spectroscopies. *J. Phys. Chem. C* **2008**, *112* (6), 2193−2201.
(49) Hu, C.; Hu, Y.; Fan, C.; Yang, L.; Zhang, Y.; Li, H.; Xie, W. Surface-Enhanced Raman Spectroscopic Evidence of Key Intermedi-

https://doi.org/10.1021/acs.nanolett.4c05658
Nano Lett. XXXX, XXX, XXX−XXX

ate Species and Role of NiFe Dual-Catalytic Center in Water Oxidation. *Angew. Chem., Int. Ed.* **2021**, *60* (36), 19774−19778.
(50) Zhang, J.; Zhang, Q. Y.; Feng, X. L. Support and Interface Effects in Water-Splitting Electrocatalysts. *Adv. Mater.* **2019**, *31* (31), 1808167.
(51) Anderson, A. B.; Roques, J.; Mukerjee, S.; Murthi, V. S.; Markovic, N. M.; Stamenkovic, V. Activation Energies for Oxygen Reduction on Platinum Alloys: Theory and Experiment. *J. Phys. Chem. B* **2005**, *109* (3), 1198−1203.
(52) Duan, Y.; Dubouis, N.; Huang, J. Q.; Dalla Corte, D. A.; Pimenta, V.; Xu, Z. C. J.; Grimaud, A. Revealing the Impact of Electrolyte Composition for Co-Based Water Oxidation Catalysts by the Study of Reaction Kinetics Parameters. *ACS Catal.* **2020**, *10* (7), 4160−4170.
(53) Huang, J.; Sheng, H.; Ross, R. D.; Han, J.; Wang, X.; Song, B.; Jin, S. Modifying Redox Properties and Local Bonding of Co_3O_4 by CeO_2 Enhances Oxygen Evolution Catalysis in Acid. *Nat. Commun.* **2021**, *12* (1), 3036.
(54) Wu, B.; Gong, S.; Lin, Y.; Li, T.; Chen, A.; Zhao, M.; Zhang, Q.; Chen, L. A Unique NiOOH@FeOOH Heteroarchitecture for Enhanced Oxygen Evolution in Saline Water. *Adv. Mater.* **2022**, *34* (43), 2108619.
(55) Xin, S.; Tang, Y.; Jia, B.; Zhang, Z.; Li, C.; Bao, R.; Li, C.; Yi, J.; Wang, J.; Ma, T. Coupling Adsorbed Evolution and Lattice Oxygen Mechanism in Fe-$Co(OH)_2/Fe_2O_3$ Heterostructure for Enhanced Electrochemical Water Oxidation. *Adv. Funct. Mater.* **2023**, *33* (45), 2305243.
(56) Tao, H. B.; Xu, Y.; Huang, X.; Chen, J.; Pei, L.; Zhang, J.; Chen, J. G.; Liu, B. A General Method to Probe Oxygen Evolution Intermediates at Operating Conditions. *Joule* **2019**, *3* (6), 1498−1509.
(57) Yang, C. Z.; Fontaine, O.; Tarascon, J. M.; Grimaud, A. Chemical Recognition of Active Oxygen Species on the Surface of Oxygen Evolution Reaction Electrocatalysts. *Angew. Chem., Int. Ed.* **2017**, *56* (30), 8652−8656.
(58) Yang, C.; Laberty-Robert, C.; Batuk, D.; Cibin, G.; Chadwick, A. V.; Pimenta, V.; Yin, W.; Zhang, L.; Tarascon, J.-M.; Grimaud, A. Phosphate Ion Functionalization of Perovskite Surfaces for Enhanced Oxygen Evolution Reaction. *J. Phys. Chem. Lett.* **2017**, *8* (15), 3466−3472.
(59) Yang, H.; Li, F.; Zhan, S.; Liu, Y.; Li, W.; Meng, Q.; Kravchenko, A.; Liu, T.; Yang, Y.; Fang, Y.; et al. Intramolecular Hydroxyl Nucleophilic Attack Pathway by a Polymeric Water Oxidation Catalyst with Single Cobalt Sites. *Nat. Catal.* **2022**, *5* (5), 414−429.
(60) Chen, R.; Hung, S.-F.; Zhou, D.; Gao, J.; Yang, C.; Tao, H.; Yang, H. B.; Zhang, L.; Zhang, L.; Xiong, Q.; Chen, H. M.; Liu, B. Layered Structure Causes Bulk NiFe Layered Double Hydroxide Unstable in Alkaline Oxygen Evolution Reaction. *Adv. Mater.* **2019**, *31* (41), 1903909.
(61) Huang, Z.-F.; Xi, S.; Song, J.; Dou, S.; Li, X.; Du, Y.; Diao, C.; Xu, Z. J.; Wang, X. Tuning of Lattice Oxygen Reactivity and Scaling Relation to Construct Better Oxygen Evolution electrocatalyst. *Nat. Commun.* **2021**, *12* (1), 3992.
(62) Ren, X.; Zhai, Y.; Yang, N.; Wang, B.; Liu, S. Lattice Oxygen Redox Mechanisms in the Alkaline Oxygen Evolution Reaction. *Adv. Funct. Mater.* **2024**, *34* (32), 2401610.
(63) Luo, X.; Zhao, H.; Tan, X.; Lin, S.; Yu, K.; Mu, X.; Tao, Z.; Ji, P.; Mu, S. Fe-S Dually Modulated Adsorbate Evolution and Lattice Oxygen Compatible Mechanism for Water Oxidation. *Nat. Commun.* **2024**, *15* (1), 8293.

https://doi.org/10.1021/acs.nanolett.4c05658
Nano Lett. XXXX, XXX, XXX−XXX